Journal of the European Ceramic Society 46 (2026) 117932

Contents lists available at ScienceDirect

Journal of the European Ceramic Society

journal homepage: www.elsevier.com/locate/jeurceramsoc

Ytterbium silicate-based environmental barrier coatings with hafnia via polymer-derived ceramic technology

Dmitrii Titov [a,b,**], Eranezhuth Wasan Awin [a,c], Stefan Schafföner [a], Günter Motz [a,*]

[a] Chair of Ceramic Materials Engineering, University of Bayreuth, Prof.-Rüdiger-Bormann-Str. 1, Bayreuth 95447, Germany
[b] Department Materials, Fraunhofer Institute for Integrated Systems and Device Technologies IISB, Schottkystr. 10, Erlangen 91058, Germany
[c] Advanced Ceramics & Composites Division, CSIR-Central Glass & Ceramic Research Institute, Kolkata, West Bengal 700032, India

ARTICLE INFO

Keywords:
Environmental barrier coatings
Polymer-derived ceramics
Rare-earth silicates
Silazanes
Silicon nitride
Self-healing coatings
Thermally grown oxide

ABSTRACT

Environmental barrier coatings (EBC) are essential to protect silicon nitride (Si_3N_4) from hot gas corrosion, enabling the utilization of Si_3N_4 in gas turbines. Otherwise the initially formed silica (SiO_2) layer degrades through reactions with the water vapor from fuel combustion. Therefore, hafnia (HfO_2) as doping additive in combination with ytterbium silicates was used to reduce the growth rate of silica and to enhance adhesion of EBCs without a bond coat. Finally, a uniform and gradient coating was generated in one stage, applied via spraying and sedimentation of a respective slurry. The in situ formed composite gradient coatings composed of HfO_2-Yb_2SiO_5/$Yb_2Si_2O_7$-Si_3N_4 without Si bond coat, exhibited excellent adhesion (42.6 ± 6.4 MPa) and high microhardness (up to 4.3 ± 0.4 GPa). The durability of these coatings was confirmed through more than 20 thermal cycling tests in the temperature range of 1200–20 °C, in which self-healing ability of cracks was proven.

1. Introduction

The profound repercussions of climatic alterations, coupled with the burgeoning necessity for carbon-neutral fuels, have engendered new challenges for researchers and engineers in the pursuit of innovative materials for aircraft jet engines. The enhancement of efficiency and the attainment of complete fuel combustion necessitate elevating the operational temperature of jet engines, alongside reductions in weight and augmentations in reliability. Nevertheless, these goals confront an impediment in the form of the thermal threshold of nickel-based superalloys, which is capped at a maximum of 900 °C [1–4]. Oxygen-free ceramics and their composite derivatives are emerging as formidable alternatives to nickel alloys. In particular, materials such as Si_3N_4 exhibit a distinctive amalgamation of characteristics, including reduced density, elevated melting point, considerable hardness, and bending strength. Si_3N_4 ceramics exhibit stability in oxidizing environments owing to the genesis of a protective SiO_2 layer during the oxidation of Si_3N_4, thereby positioning these ceramics as leading candidates for deployment in jet engine blades within the engine's high-temperature domain.

Despite their potential, the application of Si_3N_4 faces several constraints, most notably its brittleness and vulnerability to rapid degradation in environments with high-temperature water vapor. While the SiO_2 film provides a protective barrier against further oxidation in air, exposure to elevated temperatures in water vapor environments instigates an active reaction between SiO_2 and water. For instance, in scenarios where hydrogen is utilized as a fuel for jet engines, water emerges as the principal product of combustion, leading to the formation of volatile silicon hydroxide as delineated in Eqs. 1–3 [5]. Consequently, this results in the swift deterioration of the ceramics.

$$Si_3N_4 + 3/4\ O_2(g) = 3/2\ Si_2ON_2 + 1/2\ N_2(g)\uparrow \quad (1)$$

$$Si_2ON_2 + 3/2\ O_2(g) = 2\ SiO_2 + N_2(g)\uparrow \quad (2)$$

$$SiO_{2(s)} + 2\ H_2O_{(g)} \rightarrow Si(OH)_{4(g)}\uparrow \quad (3)$$

In the past two decades, considerable progress has been made in the development of a reliable environmental barrier coating (EBC) aimed at preventing hot gas corrosion. [6–10]. For an EBC to be effective, it must meet the following criteria: (1) possess a linear coefficient of thermal expansion (CTE) akin to that of the substrate to minimize thermal mismatch stresses, (2) exhibit phase stability at high temperatures, (3) maintain low thermal conductivity, and demonstrate high corrosion resistance in steam environments [11,12].

* Corresponding author.
** Corresponding author at:Chair of Ceramic Materials Engineering, University of Bayreuth, Prof.-Rüdiger-Bormann-Str. 1, Bayreuth 95447, Germany.
E-mail addresses: Dmitrii.Titov@iisb.fraunhofer.de (D. Titov), Guenter.Motz@uni-bayreuth.de (G. Motz).

https://doi.org/10.1016/j.jeurceramsoc.2025.117932
Received 11 July 2025; Received in revised form 15 October 2025; Accepted 28 October 2025
Available online 29 October 2025

Among the various materials considered for EBC, ytterbium disilicate ($Yb_2Si_2O_7$) (CTE = 3.9 × 10^{-6} K^{-1}) [13] aligns well with the required CTE of Si_3N_4 substrate (CTE = 3–5.5 ×10^{-6} K^{-1}) [7]. Within the thermal spectrum extending up to 1750 °C, only two stable ytterbium silicates are discerned: $Yb_2Si_2O_7$ (YbDS) and Yb_2SiO_5 (YbMS) (CTE = 6.3 × 10^{-6} K^{-1}) [12,14,15]. To address the slight mismatch in CTE between the substrate and the EBC of YbDS and increase adhesion, a Si bond coat is utilized. However, exposure to air and steam at elevated temperatures causes the oxidation of the Si bond coat, leading to the formation of a TGO (SiO_2) layer at the interface between the Si bond coat and EBC. While the CTE of β-cristobalite (3.1 × 10^{-6} K^{-1}) is congruent with that of the YbDS [4,7,16,17], it transforms into a denser α-cristobalite (9.6 × $10^{-5}K^{-1}$) [18] upon cooling at 277 °C, resulting in a decrease in volume by 4.9 % [19–21]. Consequently, an alternative to Si is being sought as a new material for bond coats.

The integration of HfO_2 to Si in the bond coat has garnered attention, offering improved resistance to cracking and chipping [22–26]. The HfO_2-Si, as an alternative to Si, resulted in a composite coating with superior resistance to cracking and chipping over extended test durations. Other studies also explored the use of HfO_2 for creating a TBC layer on the EBC surface, aiming to enhance the coatings' maximum operating temperature and to improve resistance to thermal shocks [27,28].

Various methods such as atmospheric plasma spraying (APS) [13,29], plasma spraying [29,30], chemical vapor deposition (CVD) [31] and physical vapor deposition [26,32] were reported for the application of EBC on Si_3N_4 substrates. In contrast, technologies based on suspensions such as the sol-gel method or polymer-derived ceramics (PDC) offer the advantage of ease in coating via spraying, dipping, or sedimentation [33–36]. Typically, preceramic polymers including silazanes, carbosilanes, and siloxanes are used as Si precursors. Subsequent heat treatment at higher temperatures led to the formation of ceramics with a high yield [37]. Recently, the production of YbDS coatings with a Si bond coat via the PDC method revealed coatings with robust adhesion (36.9 MPa), high microhardness (6.9 GPa) and the ability to withstand repeated thermal cycling. However, during the heat treatment process for coating production, unwanted SiO_2 forms along the grain boundaries of YbDS leading to the deterioration of the coatings during application [36]. To overcome the formation of SiO_2 and to enhance the durability of the coatings during their use, this research will focus on developing strategies for mitigating SiO_2 formation.

The objective of this study is to enhance the performance, physical, and chemical properties of coatings essential for their application in high-temperature steam environments. This research specifically focuses on the development and optimization of composite coatings based on YbDS doped with HfO_2 using the PDC method. A key issue addressed is the formation of the unreacted SiO_2 phase at the grain boundaries of YbDS, which negatively impacts the performance of multilayer coatings. Despite existing methods, there remains a gap in knowledge regarding effective strategies to mitigate SiO_2 formation and improve the overall durability of these coatings during use. Additionally, this study will conduct a comprehensive investigation into the structural and functional properties of the newly developed coatings to better understand their performance characteristics. Beyond Si bond coats, state-of-the-art EBC architectures increasingly employ gradient Yb_2SiO_5/$Yb_2Si_2O_7$ topcoats over Si–HfO_2 bond coats to balance steam corrosion resistance and CTE mismatch, achieving crack-free operation and parabolic TGO growth in 90 % H_2O–10 % O_2 at 1300 °C [38]. Here, we advance a complementary, Si-bond-coat-free strategy via PDC to suppress interfacial SiO_2, enable uniform or gradient HfO_2 distributions, and strengthen adhesion on Si_3N_4; we also discuss coating thickness and scale-up considerations relevant to industrial deployment.

2. Materials and methods

Fig. 1 presents the schematic diagram of the experimental protocol.

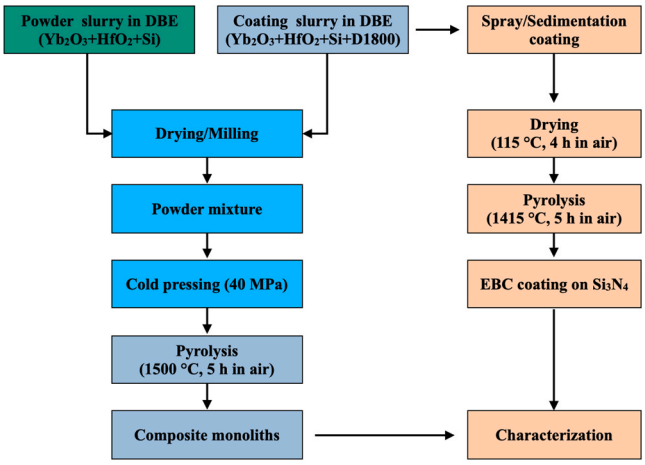

Fig. 1. Scheme of experimental methods for processing monoliths and coatings.

Comprehensive details will be described in the subsequent sections.

2.1. Materials

Ytterbium (III) oxide (Yb_2O_3) d50 = 200 nm, Reacton, 99.9 % (REO) (Alfa Aesar GmbH & Co KG, Germany) and hafnia (HfO_2) d50 = 61–80 nm, 99.9 % (IOLITEC Ionic Liquids Technologies GmbH, Germany) were used as active fillers. The oligosilazane Durazane 1800 and 3 wt% dicumyl peroxide (Merck KGaA, Germany) (D1800) served as a binder for the filler particles and as one of two sources of silicon for the development of the YbDS and YbDS/HfO_2 EBC. The oligosilazane content remained constant relative to Yb_2O_3 in all suspensions to maintain a constant solution viscosity. The reactive pyrolysis of D1800 and Yb_2O_3 in air yields mono or disilicates, depending on the Si: Yb_2O_3 ratio. The secondary Si source, elemental Si powder (Si_{pow}) grade AX 05 d50 = 4 μm (Kyocera K. K., Germany) was introduced to achieve the stoichiometric conversion of Yb_2O_3 and HfO_2 to YbDS and $HfSiO_4$ respectively [33]. The content of Si_{pow} was varied to obtain a mixture of YbMS and YbDS in the coating while keeping the oligosilazane concentration constant in all cases.

2.2. The slurry preparation

The slurry was prepared by dispersing all mentioned three powder fillers in di-n-butyl ether 99 + % (Acros Organics BVBA, Belgium) (DBE) with 4.5 wt% Disperbyk-2151 (BYK-Chemie GmbH, Germany) as a dispersing agent, based on the mass of the used powder. The HfO_2 was introduced relative to Yb_2O_3 from 1 to 15 mol%. The slurry was milled using ZrO_2 milling beads (Sigmund Lindner GmbH, Germany) in the mass ratio of 3:1 (balls: powder) to improve the homogeneity and decrease the average particle size of the fillers, thereby increasing their surface area and reactivity. Subsequently, Durazane 1800 and 3 wt% dicumyl peroxide (D1800) solution were added to the mixture. Dicumyl peroxide initiates the vinyl polymerization and hydrosilylation reactions, promoting the cross-linking of Durazane 1800 at lower temperatures and increasing the ceramic yield [39]. The molar ratio was calculated based on the ceramic yield of the oligosilazane after pyrolysis in air above 1000 °C (81 wt%). The resulting elemental composition ($SiC_{1.15}N_{0.68}O_{0.42}$) [33] according to the composition is presented in Table 1.

2.3. Processing of powders and monolithic ceramics

2.3.1. Powder preparation

For a comprehensive understanding of phase formation and the effect of additive content on coating properties, all the slurry compositions

Table 1
Composition of the slurry dispersed in di-n-butyl ether and Disperbyk-2151 mixture.

Nomenclature	Composition	Yb_2O_3, wt%	D1800, wt%	Si_{pow}, wt%	HfO_2, wt%
$YbDS_{pow}$	$Yb_2Si_2O_7$*	87.6	0	12.4	-
YbDS	$Yb_2Si_2O_7$	85.6	3.6	10.8	-
YbMS/YbDS	$1Yb_2SiO_5$: $1Yb_2Si_2O_7$	88.0	3.6	8.4	-
YbDS+ $5HfO_2$	$Yb_2Si_2O_7$ + 5 mol% HfO_2	83.2	3.6	10.8	2.3
YbDS+ $15HfO_2$	$Yb_2Si_2O_7$ + 15 mol% HfO_2	79.0	3.6	10.0	7.4
YbMS/YbDS+ $15HfO_2$	$1Yb_2SiO_5$: $1Yb_2Si_2O_7$ + 15 mol% HfO_2	81.0	3.6	7.7	7.7

* Slurry without precursor D1800

were air-dried for 24 h to remove the solvent di-n-butyl ether. Subsequent polymerization of D1800 was carried out at 115 °C in air for 4 h. The resultant powders were grounded in a vibratory disc mill Pulverisette 9 (Fritsch GmbH, Germany) for 60 s, yielding a homogeneous powder with reduced particle size.

2.3.2. Cold pressing of monolithic ceramics

The monolithic ceramics were obtained by uniaxial cold pressing the dried powders in a stainless-steel mold at 40 MPa with approximate dimensions of Ø 12 × 3 mm, followed by pyrolysis in air at 1500 °C for 5 h in a box furnace (Nabertherm GmbH, Germany). The effect of HfO_2 and D1800 concentration on the microstructural and phase composition of the monolithic ceramics was thoroughly investigated.

2.4. Coatings

Si_3N_4 substrates with the addition of a sintering additive, consisting of a mixture of Y_2O_3, MgO and Al_2O_3 (SNPU FCT Ingenieurkeramik GmbH, Germany) were used as substrates with sizes of 10x10x2 mm and 30x25x5 mm. The substrates were prepared by hot pressing and then precisely cut to the required dimensions using a laser machine. The cutting process resulted in residual material, referred to as "dross," which was subsequently removed by grinding with SiC abrasive paper (grid size P80). Subsequently, the substrates were cleaned in acetone using an ultrasonic bath for 20 min.

The dried substrates were coated using two different methods. In the first approach, the slurry was sprayed, using a 781S spray gun (Nordson Deutschland GmbH, Germany). In the second method, the slurries were placed at the bottom of the evaporation cups and the slurry was poured over them to achieve a coating thickness of 50–100 μm. The substrates remained within the cups until complete evaporation which typically occurred within 24 h. This was followed by a drying and a polymerization process at 115 °C for 4 h in both cases with subsequent pyrolysis carried out in air at 1415 °C for 5 h. In the context of thickness effects, the chosen 50–100 μm range reflects a trade-off: thicker EBCs improve vapor infiltration resistance but amplify thermal mismatch stresses; gradient architectures mitigate this trade-off by distributing composition and stiffness across the thickness [38]. For scale-up, both spraying and sedimentation are compatible with larger areas, but gradient control via sedimentation requires consistent slurry rheology and particle-size distributions to ensure reproducible layer stacking.

2.5. Analysis and characterizations

2.5.1. Pyrolysis behavior of the composite powders

The study of the pyrolysis process and the corresponding mass changes depending on the additive concentration was carried out using thermogravimetric analysis (TGA) on an STA 449 F5 Jupiter (Netzsch GmbH & Co. Holding KG, Germany). The measurements were performed up to 1500 °C at 10 K min^{-1} in a synthetic air atmosphere (80/20 vol% N_2/O_2).

2.5.2. Monoliths: composition and microstructure

The phase composition analysis of the sintered monoliths at 1500 °C for 5 h in air was carried out by X-ray diffractometry (XRD) (D8 ADVANCE, Bruker AXS, Germany) using monochromatic CuKα radiation. The resulting diffractograms were evaluated using the PDF-4 + 2020 structural database. The influence of the HfO_2 addition on the sintering process was analyzed using a dilatometer 402E Netzsch (Netzsch GmbH & Co. Holding KG, Germany). Additionally, the microstructure of transverse polished sections of the prepared monoliths was analyzed using scanning electron microscopy (SEM, Gemini Sigma 300 VP, Carl Zeiss AG, Germany), coupled with an EDAX Octane Elect Silicon Drift Detector (SDD) for energy-dispersive X-ray spectroscopy (EDS).

2.5.3. Properties of the coating system on Si_3N_4

The coating's microstructure and phase composition were examined using SEM and EDS. The crystalline phases were determined through XRD measurements on the surface of the coated samples. Microhardness measurements were performed using a Fischerscope HM2000 (Helmut Fischer GmbH, Germany) with a maximum applied load of 500 mN (HV 0.1). Each sample was tested 20 times across the entire surface, and the resulting microhardness values were calculated as the mean value. Coating adhesion properties were measured using the pull-off method with a PosiTest AT-A (DeFelsko Corp., USA) by ASTM D4541. Dollies of Ø 10 mm were glued to the coating surface using a two-component epoxy resin Loctite EA 9466 (Henkel Central Eastern Europe GmbH, Austria). The resin was cured at 110 °C for 1 h in air before conducting the pull-off test with a constant rate of force application of 1 MPa•s^{-1}. The values obtained were averaged over 3 measurements. The thermal cycling stability of coated substrates was evaluated by subjecting the coated samples to a series of 20 cycles for 1 h in an N41/H chamber furnace (Nabertherm GmbH, Germany) pre-heated at 1200 °C, followed by quenching in a water bath at 20 °C. After each cycle, the samples were dried at 110 °C for 30 min in a Nabertherm LE 14/11 chamber furnace before the subsequent test.

3. Results and discussion

3.1. Pyrolysis behavior of slurry and microstructure of $Yb_2Si_2O_7$ + HfO_2 monoliths

In a multi-component system, the presence of two sources of free silicon (Si_{pow} and D1800), can lead to distinct reactions and different coating properties upon interaction with HfO_2 and Yb_2O_3. Hence, it is important to evaluate the interaction between the individual components. The previous study [36] showed that Si_{pow} oxidises at 750 °C, forming an amorphous and dense SiO_2 scale thereby preventing the complete rapid oxidation of Si_{pow}. Conversely, D1800 degrades at temperatures above 400 °C, leading to a weight loss that occurs up to 750 °C, where SiO_2 begins to form. The resulting passivation layer impedes the complete removal of carbon and nitrogen, forming SiO_2 around an amorphous ceramic with the composition of $SiC_{1.15}N_{0.69}O_{0.41}$ after pyrolysis [33].

In this study, we analyzed the mass change of HfO_2 and Yb_2O_3 with Si_{pow} / D1800. In the TGA measurements, a slight increase in mass (0.5–1 %) was observed for Yb_2O_3+D1800 at 1050 °C, unlike for the HfO_2+D1800 composition. This increase was attributed to the formation of YbMS due to the reaction of Yb_2O_3 with D1800. Subsequently, the mass of both mixtures remained stable up to 1500 °C.

When interacting with Si_{pow}, oxides behaved differently. HfO_2+Si_{pow} and Yb_2O_3+Si_{pow} mixtures remained stable until 750 °C, followed by a mass increase. At 1050 °C, the mass of the Yb_2O_3+Si_{pow} sample increased, linked to the formation of YbMS. An intensive weight increase was also noted for the Yb_2O_3+Si_{pow} sample at temperatures above 1400 °C, attributed to the formation of YbDS due to the interaction of YbMS with SiO_2. This reaction was not observed for HfO_2+Si_{pow}, indicating no reaction between HfO_2 and SiO_2 under these conditions.

Differential scanning calorimetry (DSC) analysis revealed differences in the reactions of Yb_2O_3 and HfO_2 with D1800/Si_{pow}. A peak corresponding to YbMS formation was observed at 1050 °C for Yb_2O_3+D1800 as well as Yb_2O_3+Si_{pow}. However, at 1400 °C, there was no YbDS formation for Yb_2O_3+D1800, indicating the formation of a passivation YbMS layer over Yb_2O_3, preventing the complete reaction of Yb_2O_3. For HfO_2+D1800, a peak at ~1150 °C was associated with the formation of hafnon ($HfSiO_4$) (see supplementary materials Fig. S1).

In the case of the Yb_2O_3+Si_{pow} powder, the DSC revealed the formation of YbDS indicating a crucial step in the material transformation process. However, a more comprehensive understanding of the material's behavior is necessary, particularly regarding its shrinkage tendencies, which may provide valuable insights into its structural stability and performance. Hence, monolithic ceramics were prepared enabling a more comprehensive assessment of its structural dynamics and stability. Additionally, the detailed examination of the influence of varying HfO_2 contents (5 and 15 mol%) on the Yb_2O_3+Si_{pow} composition was investigated elucidating the intricate relationship between the components and their resulting properties.

Dilatometric analysis of monolithic Yb_2O_3+Si_{pow} and their composites with varying HfO_2 contents indicated that the YbMS formation decreases as the amount of HfO_2 increases. This finding is significant for sintering coatings, as it helps mitigate high expansion transformation effects. The composites containing 5 mol% HfO_2 exhibited the most significant shrinkage. Analyzing the shrinkage curve's first derivative, which represents the shrinkage rate, showed a gradual decrease in this rate with increasing HfO_2, particularly evident after YbDS formation (above 1415 °C). Yb_2O_3+Si_{pow} with addition of 5 mol% HfO_2 displayed continuous shrinkage, suggesting incomplete ceramic densification up to 1500 °C. Continuous shrinkage in Yb_2O_3+Si_{pow} is likely due to YbDS grain coarsening, a process that is inhibited by the addition of HfO_2 (see supplementary materials Fig. S2).

Fig. 2 presents the X-ray diffractograms of monolithic $YbDS_{pow}$, $YbDS_{pow}$+ 5HfO_2, and $YbDS_{pow}$+ 15HfO_2, all sintered at 1500 °C in air. XRD measurements of these ceramic composites revealed that an increase in HfO_2 concentration leads to a reduction in the YbMS phase. The presence of the HfO_2 phase was observed in the $YbDS_{pow}$+ 15HfO_2 monolithic ceramics. Notably, in the $YbDS_{pow}$+ 5HfO_2 composition, traces of YbMS persisted alongside hafnium silicate ($Hf_{0.75}Si_{0.25}O_2$). Furthermore, the formation of the ytterbium hafnate phase was also noted only in the $YbDS_{pow}$+ 15HfO_2 monoliths. It is important to highlight that as the concentration of HfO_2 in the composition increased, so did the content of SiO_2 in the form of α-cristobalite. Given that the system's components were chosen to form YbDS and hafnon, it appears that not all SiO_2 reacted with the HfO_2 [40]. This assumption also explains the absence of YbMS in the YbDS+ 15HfO_2 composite, as there was an excess of SiO_2 in the system, leading to the complete reaction and formation of YbDS.

To understand the impact of the two different silicon sources, Si_{pow} and D1800, on the Yb_2O_3 and HfO_2 powders, the microstructures of the respective monoliths of Yb_2O_3+ 15HfO_2+Si_{pow} and Yb_2O_3+ 15HfO_2+Si_{pow}+D1800 were analysed (Fig. 3). As the micrograph of $YbDS_{pow}$ (Fig. 3a) and $YbDS_{pow}$+ 15HfO_2 (Fig. 3b) show an increase in the concentration of HfO_2 led to the appearance of a large amount of SiO_2. It can be assumed that the appearance of silica was caused by the low reactivity of HfO_2, which was discussed above. For the sample without the addition of HfO_2, there almost no SiO_2 was presented. These data are consistent with the work reported by Zhang et al. [41]. They demonstrated that after 200 h of heat treatment at 1475 °C, the $HfSiO_4$ peak became more intense than the HfO_2 peak at the HfO_2/SiO_2 component ratio of 5/5. It was noted that the formation of hafnon at a HfO_2/SiO_2 mol ratio of 7/5 needed a longer heat treatment time than for a ratio of 5/5. From these findings, it should be concluded that when obtaining a coating for 5 h at 1415 °C, it is impossible to obtain 100 % $HfSiO_4$ yield. To achieve a silica content reduction in the coating, it was necessary to reduce the amount of the Si_{pow} filler, which

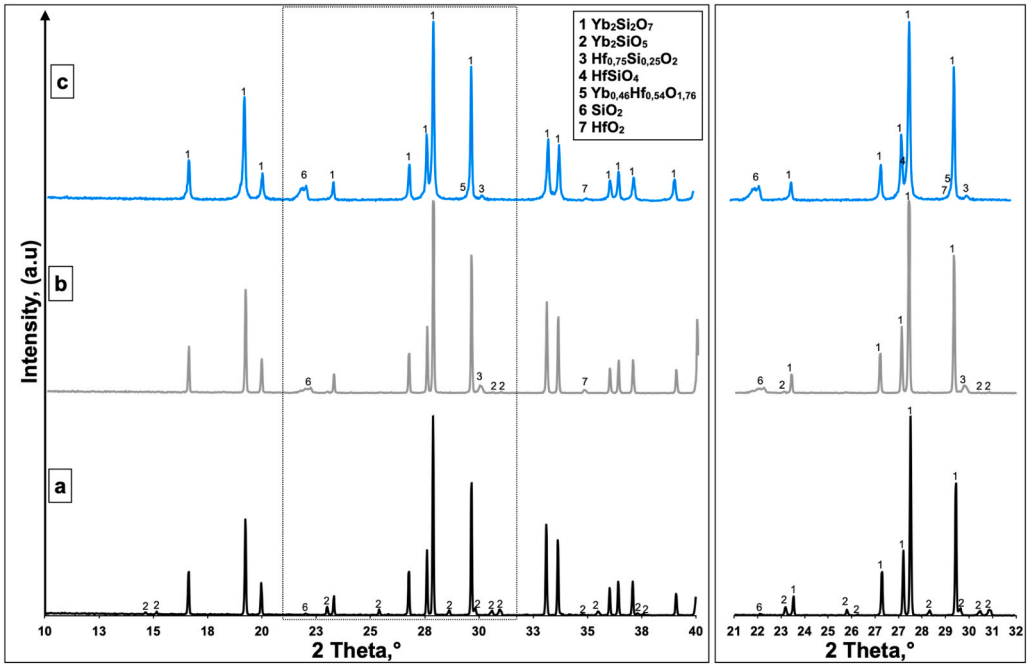

Fig. 2. XRD patterns of monolithic ceramics: a –pure $YbDS_{pow}$; b – $YbDS_{pow}$+ 5HfO_2; c – $YbDS_{pow}$+ 15HfO_2 sintered at 1500 °C 5 h in air. 1 – $Yb_2Si_2O_7$ peaks (PDF 00–025–1345), 2 – Yb_2SiO_5 peaks (PDF 00–040–0365), 3 – $Hf_{0.75}Si_{0.25}O_2$ peaks (PDF 04–002–0611), 4 – $HfSiO_4$ peaks (PDF 00–008–0345), 5 – $Yb_{0.46}Hf_{0.54}O_{1.76}$ peaks (PDF 04–002–2733), 6 – SiO_2 peaks (PDF 04–013–9484), 7 – HfO_2 peaks (PDF 04–002–0037).

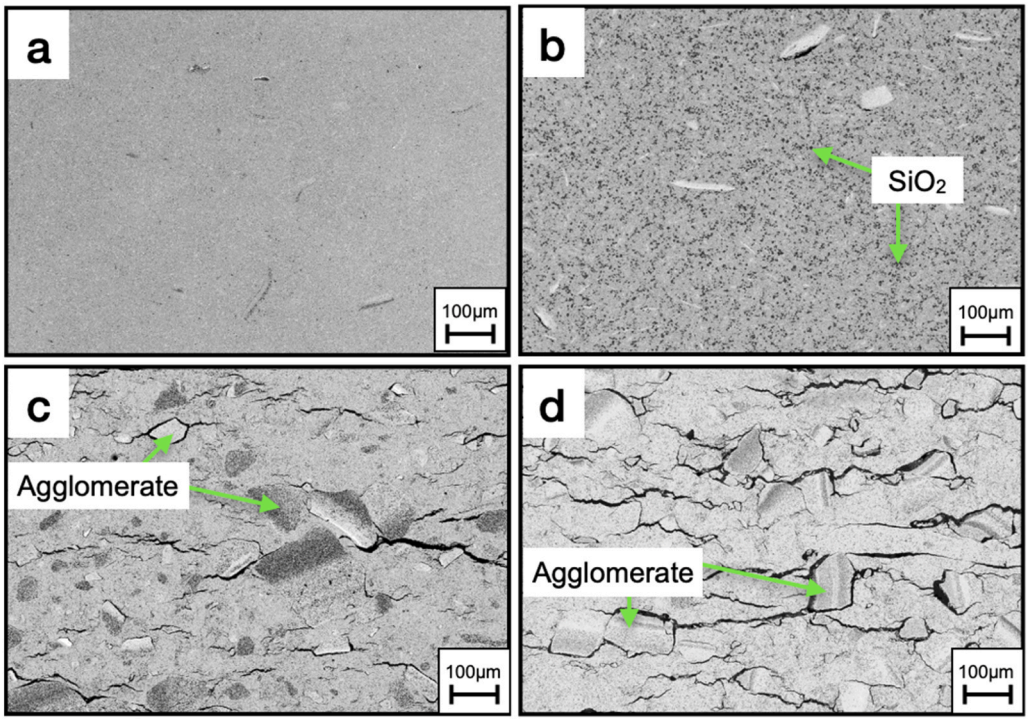

Fig. 3. SEM of the cross-section of monoliths: a – $YbDS_{pow}$; b – $YbDS_{pow}$+ 15HfO_2; c – YbDS, d – YbDS+ 15HfO_2.

goes to the formation of hafnon by 50 % because all silica is not completely consumed during sintering and hurts the protective properties of the YbDS coating during hot gas corrosion.

Fig. 3c-d shows similar ceramic composites with the addition of both Si_{pow} and D1800. The non-uniformity and the presence of a large amount of SiO_2 distributed throughout the volume were observed. The SEM analysis confirmed the hypothesis about the formation of a passivation layer on the surface of Yb_2O_3 and HfO_2 agglomerates due to covering with D1800.

A detailed SEM/EDS analysis of the agglomerate of YbDS+ 15HfO_2 is shown in Fig. 4. In the center of the agglomerate, unreacted particles of HfO_2 and YbMS were found. The core was surrounded by dense layers of YbMS and YbDS with a thickness of about 5–8 μm. The outer region was filled with a mixture of YbDS and SiO_2. Due to the difference in the CTE of the agglomerate and the main matrix of the monolith, cracks occurred after sintering. Accordingly, because part of the Yb_2O_3 did not react to form YbDS, an excess of silica remains in the monolith, which reduces the thermo-mechanical properties of ceramics.

Based on the fact that agglomerates were formed in monoliths only in the presence of D1800, it can be assumed that the mechanism of their formation is associated with the capture of HfO_2 and Yb_2O_3 particles by D1800. Since nanosized particles have a high surface energy, they form agglomerates which are surrounded by the precursor. During the pyrolysis, SiO_2 is formed from the precursor, which has a high reactivity. It reacts on the surface of the agglomerate with Yb_2O_3, forming a dense passivation layer of YbDS. This layer prevents further contact of unreacted ytterbia with free SiO_2. For this reason, the phase equilibrium shifted in the monolith composition and a large amount of SiO_2 remains in the matrix due to an excess of unreacted Si_{pow} filler, whereas unreacted HfO_2 and Yb_2O_3 were located inside the agglomerates

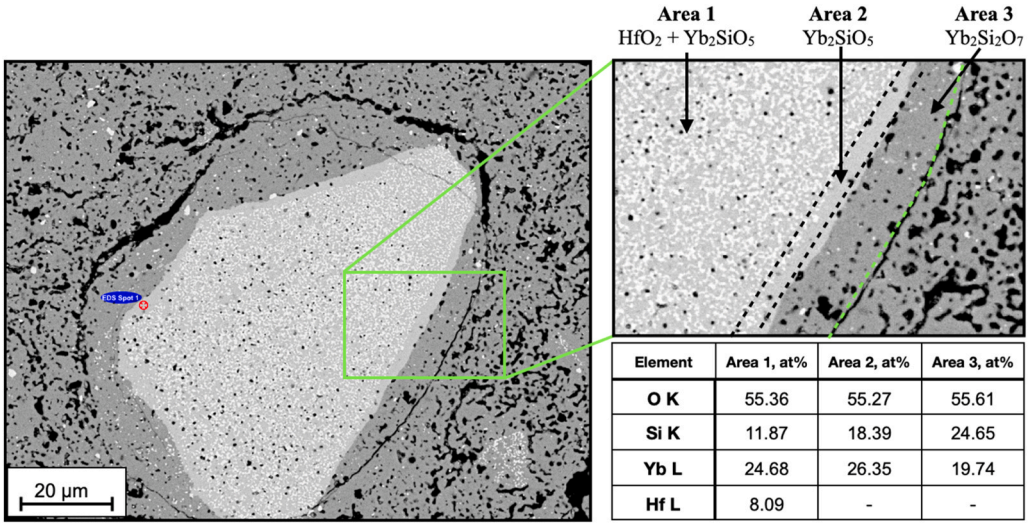

Element	Area 1, at%	Area 2, at%	Area 3, at%
O K	55.36	55.27	55.61
Si K	11.87	18.39	24.65
Yb L	24.68	26.35	19.74
Hf L	8.09	-	-

Fig. 4. SEM/EDS of the cross-section of an agglomerate within the YbDS+ 15HfO_2 monolithic ceramic.

("capsules"). Due to the low reactivity of HfO_2, no encapsulated effect was found consisting of a $HfSiO_4$ passivation layer. In all cases, the outer dense layer of the "capsule" consisted exclusively of YbDS. Even so, Anton et al. reported the formation of a passivation layer consisting of $HfSiO_4$ around HfO_2. However, this passivation layer required an exposure time of up to 200 h [26]. The proposed mechanism for the formation of "capsules" is shown in Fig. 5.

3.2. Properties of coating system based on $Yb_2Si_2O_7$

3.2.1. Principles of silicon oxide formation on $Yb_2Si_2O_7$ grain boundaries

The previous study from our group demonstrated that in the case of the sintering composition of the Si: Yb (2:1) coating system, to obtain pure YbDS EBC, a significant amount of SiO_2 was formed along the grain boundaries [36]. The excess of SiO_2 along the grain boundaries of the coating can occur due to three reasons. The first reason could have been the formation of a TGO layer on the Si_3N_4 surface. The second and third possibility, on the other hand could be the oxidation of the Si bond coat or an incomplete reaction between silicon oxide and ytterbium oxide, resulting in the formation of ytterbium silicates. The unreacted SiO_2 was distributed along the grain boundaries of ytterbium silicate upon the sintering.

To analyse the assumptions mentioned above, we applied Yb_2O_3+Si_{pow}+D1800 coatings on the Si_3N_4 substrate without a Si bond coat using spraying and sedimentation techniques. Fig. 6 shows SEM micrographs of YbDS and YbMS/YbDS coatings pyrolyzed at 1415 °C. The filler was added in two different quantities to achieve pure YbDS and YbMS/YbDS in the coatings, respectively. This allowed to examine the effect of reducing the Si_{pow} filler amount towards the occurrence of SiO_2 along the ytterbium silicate grain boundaries. Secondary electron (SE) images were used to distinguish the SiO_2 among the YbDS grains and backscattered electrons (BSE) to see the phase distribution of YbMS and YbDS in the coating.

Fig. 6a shows that in the case of the YbDS coating, SiO_2 was present at the grain boundaries. Decreasing the Si_{pow} filler content resulted in the complete disappearance of SiO_2 along the grain boundaries, a reduction in grain size and the formation of pores (Fig. 6b). The average grain size of the coatings was found to be 1–10 μm and 0.5–3 μm for YbDS and YbMS/YbDS, respectively. It was observed that the presence of the YbMS phase inhibited the YbDS grain growth. BSE micrographs as shown in Fig. 6c and d reveal the phase distribution of YbDS and YbMS demonstrating a substantial number of pores on the surface. These pores were filled with SiO_2 in the presence of an excess Si_{pow} in the case of YbDS coating, while the deficit of filler led to the formation of new pores.

The dilatometric (DIL) and thermogravimetry (TG) curves of pure silicon, Yb_2O_3+Si_{pow} and Yb_2O_3+Si_{pow}+D1800 composites are shown in Fig. 7. It was found that at the first stage, Si_{pow} began to actively gain weight due to the oxidation above 800 °C. A similar trend was also observed for Yb_2O_3+Si_{pow} and Yb_2O_3+Si_{pow}+D1800 composites. In the second stage, the increase in mass at 1050 °C might have been the result of the silicon oxidation and the formation of YbMS. A comparison of the dilatometry and TG curves revealed that the process of silicon oxidation and the formation of ytterbium monosilicate occurred at a significantly lower temperature than the formation of YbDS and the full densification of the coating (up to 1500 °C), the third stage. It can be concluded that a temperature increase, the Si_{pow} gets oxidised and reacts with Yb_2O_3 resulting in the formation of YbMS and the shrinkage process starts (above 1250 °C). Thus, the presence of a Si bond coat will always lead to the formation of a TGO layer and the appearance of excess SiO_2 along the boundaries of YbDS grains. Hence, the only possibility of obtaining a coating without SiO_2 is to apply the deficit of Si filler coating on the substrate without a Si bond coat.

Furthermore, when the Yb_2O_3+Si_{pow}+D1800 slurry was applied as a coating on the Si_3N_4 substrate, the Si_3N_4 substrate oxidized and formed a thin layer of SiO_2 (TGO) during the densification of the coating. The aforementioned TGO layer reacted with Yb_2O_3 to form YbMS. Upon further increase in temperatures, YbMS converted to YbDS owing to the availability of SiO_2. The excess SiO_2 was distributed along the grain boundaries of YbDS. The entire process is schematically represented in Fig. 8.

3.2.2. $Yb_2Si_2O_7$ + HfO_2 coatings

As explained, in the introduction, HfO_2 is used as an additive for the bond coat. However, there is no data on how the properties of YbDS EBC change in which the HfO_2 additive is evenly distributed in the EBC. Fig. 9 illustrates the SEM micrographs of the Yb_2O_3+Si_{pow}+D1800 coatings surfaces with varying HfO_2 dopant content (ranging from 0 to 15 mol%), which were obtained through the spraying method and pyrolyzed at 1415 °C. The SEM micrographs reveal that an increase in the HfO_2 content effectively hinders the grain growth of YbDS. The shape and average grain size are detailed in Table 2.

The surfaces of the coatings with HfO_2 additions still exhibited the presence of SiO_2 at the YbDS grain boundaries. However, as the concentration of HfO_2 increased, the grain size of the YbDS decreased, leading to an increase in the coating's density.

EDX and XRD analysis of the coating surface with the highest content of hafnium oxide (15 mol%) showed the presence of pure HfO_2 (1.5 %) and SiO_2 (6.1 %) dispersed in the continuous matrix of ytterbium disilicate (85.6 %). XRD confirmed the presence of a silica phase at the grain boundaries and the presence of traces of ytterbium hafnate. Based on theoretical calculations, the content of the hafnon phase should have been 8.5 wt% which is 30 % higher than the measured one. By contrast, the measured content of ytterbium disilicate was only 7 % lower than the calculated amount. This difference once again confirmed the low reactivity of hafnium oxide when interacting with silicon oxide (Fig. 10).

In our experimental work, we propose the development of a coating with a high content of hafnium oxide on the surface. This coating structure is anticipated to enhance the heat resistance and durability due to the low thermal conductivity of hafnium oxide. Specifically, heat resistance refers to the coating's ability to withstand high temperatures without degradation. In the following subsection, we will examine the properties of coatings with both uniform and gradient distributions of hafnium oxide in environmental barrier coatings (EBCs).

3.2.3. Sprayed and sedimented $Yb_2Si_2O_7$+HfO_2 EBCs

Recent studies suggest to enhance the resistance of coatings in a hot gas corrosion environment, it is necessary to either modify Si bond coat with hafnon to decrease TGO layer growth [29,4130,40] or explore alternative approaches. Deijkers et al. proposed the use of HfO_2 as TBC on the

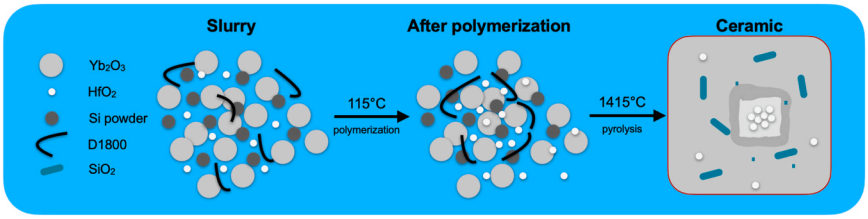

Fig. 5. Schematic mechanism of the formation of agglomerates.

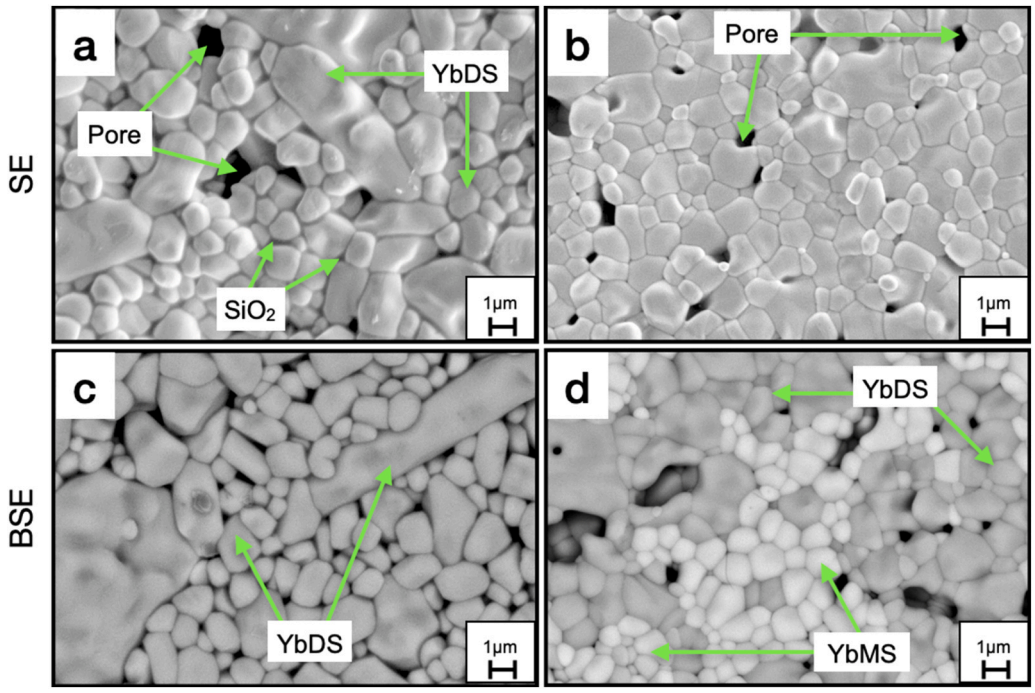

Fig. 6. SEM micrographs of the surface coatings: a –YbDS; b - YbMS/YbDS in secondary electron (SE) mode and c –YbDS; d - YbMS/YbDS in backscattering electrons (BSE) mode.

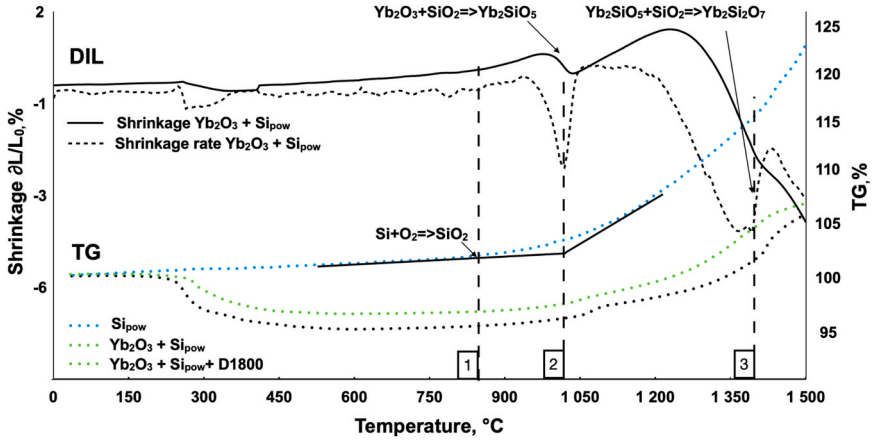

Fig. 7. Comparing dilatometry (DIL) and thermogravimetry (TG) curves to understand the process of the SiO_2 formation on the YbDS boundaries.

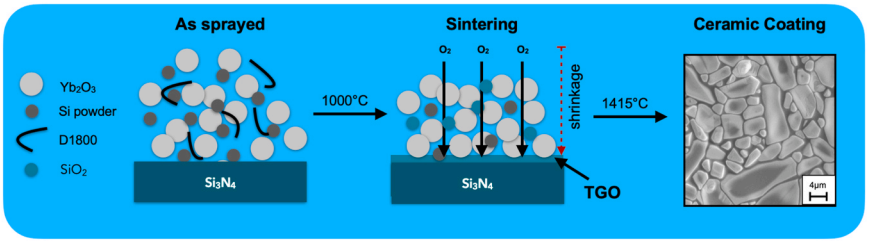

Fig. 8. Schematic of excess SiO_2 formation at the YbDS grain boundaries.

YbDS surface to increase the heat resistance of the coating [42]. However, applying these coatings on substrates involved the atmospheric plasma spraying (APS) technique which was found to be challenging for multilayer coatings because of the reactions between layers and the fluorite formation. In this context, in the present study coatings obtained through the polymer-derived ceramics (PDC) technique using both the sedimentation and spraying method were compared.

Unlike the spraying method, which was discussed above, the sedimentation method facilitated the achievement of a layer-by-layer or gradient coating. The sedimentation process is influenced by viscosity and particle size, which plays a critical role in the coating formation. On the one hand, the presence of D1800 in the suspension changed the

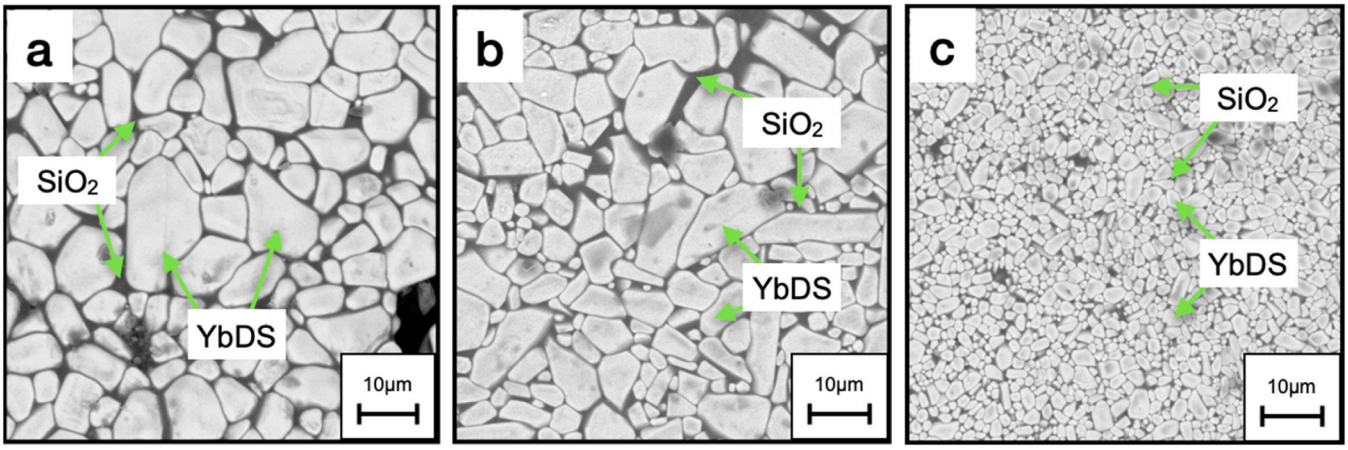

Fig. 9. Effect of HfO_2 doping content on the YbDS coating microstructure: a – YbDS, b – YbDS+ 5HfO_2, c – YbDS+ 15HfO_2.

Table 2
The grain size and shape of the YbDS and YbDS with HfO2 additive coatings obtained by spraying and pyrolyzing at 1415 °C for 5 h in air.

Coating	Grain size, μm	Shape
YbDS	7–15	Oblong
YbDS+ 5HfO_2	3–15	Oblong and round
YbDS+ 15HfO_2	0.5–2	Round

viscosity of the solution. On the other hand, due to the higher density, the first Yb_2O_3 settled on the substrate surface, followed by the joint sedimentation of Si_{pow} and Yb_2O_3, followed by finely dispersed HfO_2. HfO_2 sedimentated as the top layer on the Si_3N_4 substrate. Subsequent sintering led to the formation of a coating consisting of YbDS with the addition of HfO_2, the concentration of which increased from the substrate to the coating surface resulting the gradient EBC.

Fig. 11a and b depict coatings from Yb_2O_3+ 15HfO_2+Si_{pow}+D1800 suspension obtained by spraying and sedimentation methods, respectively. The EDX analysis of coatings obtained using spraying confirmed a uniform distribution of HfO_2 throughout the entire coating volume (Fig. 11a). The coating itself was found to be dense and uniform. However, due to the growth of TGO, the EBC peeled off from the substrate.

In contrast to the sprayed coating, the EBC from the sedimentation method adhered tightly to the substrate and consisted of three main layers with boundaries in between them. During the sedimentation of the slurry on the substrate, the phase equilibrium in the system shifted, leading to an enrichment of Yb_2O_3 and a deficit of Sipow closer to the substrate surface. Sintering of the coating caused to the oxidation of the Si_3N_4 substrate surface because until fully density of the coating is reached, it is permeable to oxygen and a SiO_2 layer forms on the surface is a result. Due to the deficit of the Si_{pow} in the sedimented slurry close to the substrate, the TGO reacted with Yb_2O_3 to form a thin YbDS boundary layer at the EBC-Si_3N_4 interface. In this case, the EBC is obtained without TGO and isn't chipping. The first layer consisted of a mixture of YbMS and Yb_2O_3, whereas the second layer was enriched with SiO_2. As a result, the main phases are YbDS and SiO_2, with the latter being 20 μm thick. The top layer consisted more of HfO_2 and YbDS approximately in the ratio of 3:1 with a thickness of about 4–6 μm according to the EDS.

The multilayer microstructure prevented the coating from cracking, featuring a TBC-like top layer that protects the EBC layer from overheating and damage as it was proposed by Deijkers et al. [42]. Additionally, the contact layer with the substrate exhibited a high adhesion (Table 3) due to the absence of a TGO layer between the coating and the substrate.

Table 3 illustrates the adhesion values of the coatings. It demonstrates that the YbDS coatings without HfO_2 additive exhibited minimal adhesion to the Si_3N_4 substrate due to the growth of the thermally grown oxide (TGO), resulting in poor adhesion. However, the introduction of HfO_2 significantly increased the adhesion values (30 and 38 MPa for the sprayed and sedimented ion coatings, respectively). Since the HfO_2 additive was introduced into a suspension with a deficiency of Si, we hypothesize that the increase in adhesion may be attributed to several factors. Firstly, the partial formation of hafnone and hafnium silicates

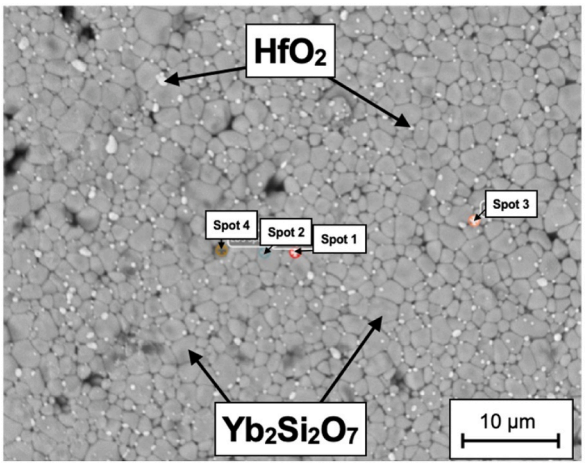

EDX data

SPOT 1/3	Weight %	Atomic %	Error %
C K	32.93	68.97	10.84
O K	15.03	23.63	10.88
Yb L	14.39	2.09	15.09
Hf L	37.66	**5.31**	10.99

SPOT 2/4	Weight %	Atomic %	Error %
C K	34.21	62.34	11.06
O K	20.26	27.71	10.63
Si K	6.42	5.00	6.92
Yb L	37.01	4.68	8.07
Hf L	2.09	0.26	56.84

XRD data

$Yb_2Si_2O_7$	$HfSiO_4$	$Hf_{0,75}Si_{0,25}O_2$	$Yb_{0,46}Hf_{0,54}O_{1,76}$	HfO_2	SiO_2
85,6 %	6,1 %	0,6 %	0,2 %	1,5 %	6,1 %

Fig. 10. BSE/EDX surface chemistry compared with XRD data of YbDS+ 15HfO_2 coating.

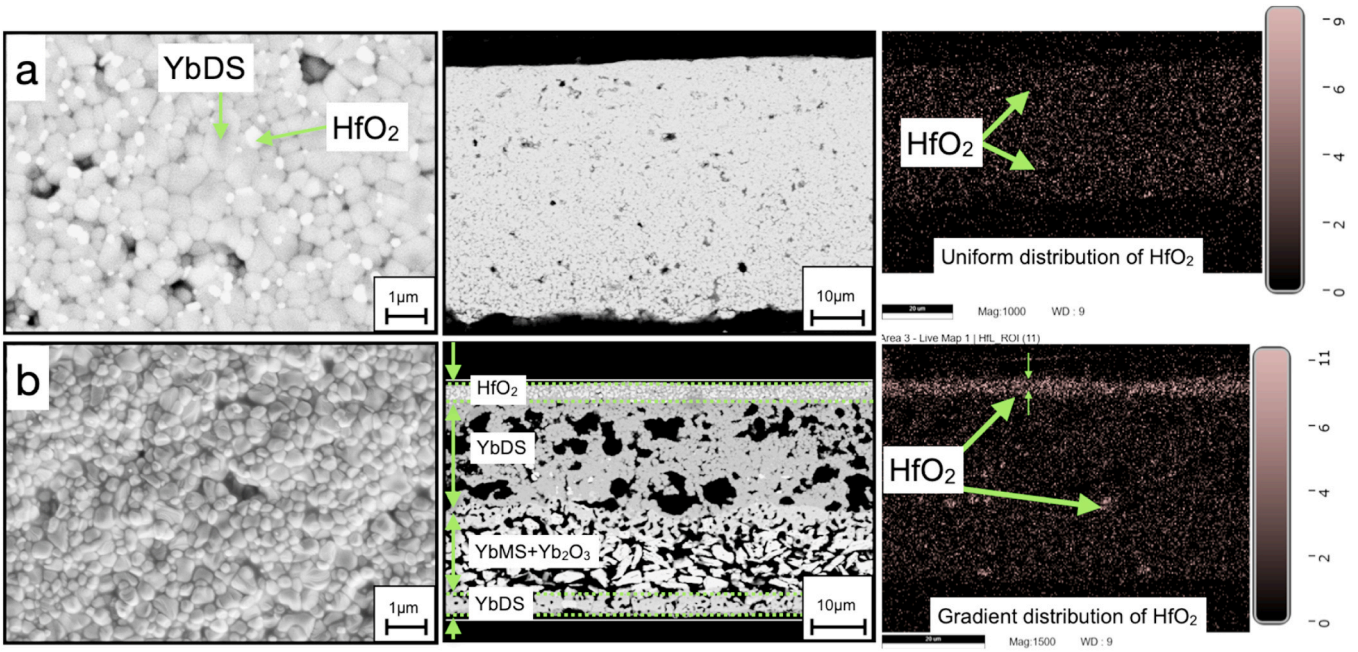

Fig. 11. SEM/EDX of YbDS+ 15HfO_2 ceramic coatings obtained via a – spraying and b – sedimentation methods.

Table 3
The adhesion values of the EBC obtained by spraying and sedimentation techniques, MPa.

	Spraying	Sedimentation
YbDS	0	0
YbDS+ 15HfO_2	30.2 ± 4.5	38.0 ± 5.6
YbMS/YbDS+ 15HfO_2	42.6 ± 6.4	40.1 ± 6.0

likely contributed to this improvement. Consequently, the Yb_2O_3-2SiO_2 system shifts towards an excess of ytterbium oxide, which may react with the TGO on the surface of the Si_3N_4 substrate.

Secondly, the oxidation reaction of the Si_3N_4 proceeded with a decrease in volume by ΔV_1 = -36.6% (Eq. 4). If it is assumed that all the formed TGO reacts with HfO_2 and YbMS to form hafnone and YbDS, an increase in volume by about ΔV_2= 12.8% and ΔV_3= 10.1% would occur (Eqs. 5 and 6). Since the studies [25,32,40,41] described above have shown that the reaction of HfO_2 with SiO_2 proceeds only partially, and the TGO layer on the surface is very thin. Thus, the volume changes seem to completely compensate for each other.

$$\Delta V_1 = \left(\frac{V_{SiO_2}}{V_{Si_3N_4}} - 1\right) \times 100\% = \left(\frac{25.77}{40.69} - 1\right) \times 100\% = -36.6\% \quad (4)$$

$$\Delta V_2 = \left(\frac{V_{HfSiO_4}}{\frac{1}{3}V_{Si_3N_4} + V_{HfO_2}} - 1\right) \times 100\%$$

$$= \left(\frac{38.78}{\frac{1}{3} \times 40.69 + 20.82} - 1\right) \times 100\% = +12.8\% \quad (5)$$

$$\Delta V_3 = \left(\frac{V_{Yb_2SiO_7}}{\frac{1}{3}V_{Si_3N_4} + V_{Yb_2SiO_5}} - 1\right) \times 100\%$$

$$= \left(\frac{83.58}{\frac{1}{3} \times 40.69 + 62.36} - 1\right) \times 100\% = +10.1\% \quad (6)$$

where ΔV_1, ΔV_2 and ΔV_3 are the changes in molar volume as a result of the oxidation reaction of Si_3N_4, the formation of hafnone and YbDS, respectively.

Thirdly, the reaction between HfO_2 and TGO forms hafnon. Its $CTE_{HfSiO4} = 3.6–4.17 \times 10^{-6}\,K^{-1}$ is similar tot he CTE of Si_3N_4, reducing the thermal stress on the EBC-substrate boundaries during cyclic oxidation of EBC, as was previously demonstrated by Zhang et al. [29].

Thus, a reduction in the Si_{pow} content in the initial suspension should theoretically enhance the coating adhesion. This is because the Yb_2O_3 and HfO_2 in the coating react with the SiO_2 on the substrate surface rather than with the Si_{pow}. This results in the minimizing the TGO layer and promoting a tighter EBC-substrate contact. Experimental data validated this hypothesis, as the YbMS/YbDS+ 15HfO_2 EBC had the maximum achieved adhesion (40–43 MPa).

Fig. 12a and b depict the SEM micrographs of YbMS/YbDS+ 15HfO_2 coatings obtained using the spraying and sedimentation methods, respectively. The EDX mapping of the oxygen content revealed a highly dense contact between the coating and the substrate. This observation suggests the presence of a thin TGO layer with a thickness of less than 1μm. Furthermore, the presence of cracks in the coating did not affect the thickness of the TGO layer. When a crack was formed, it was filled with SiO_2, which subsequently reacted with YbMS, leading to the formation of YbDS resulting in the crack healing.

The microhardness of the coatings obtained using the spraying and sedimentation method is tabulated in Table 4. A decrease in microhardness was observed when the YbMS phase was present, regardless of the method of coating application. The lower microhardness observed for the YbMS/YbDS+ 15HfO_2 coating could be attributed to the presence of pores in the coating [36]. Notably, the microhardness of the sprayed coatings was higher than that of the sedimentation coatings.

The thermal shock resistance of the obtained coatings was evaluated using a thermocyclic test in a temperature range from 1200 to 20 °C. The YbMS/YbDS+ 15HfO_2 coating system demonstrates high resistance to thermal shock. This can be attributed to two factors: firstly, the identical CTE of the coating ($CTE_{YbMS/YbDS}$=5.1 × 10^{-6} K^{-1}, CTE_{HfSiO4} = 3.6–4.17 ×10^{-6} K^{-1}, CTE_{HfO2}=8.4 ×10^{-6} K^{-1}) and the substrate (CTE_{Si3N4}=3–5.5 × 10^{-6} K^{-1}); secondly, the influence of the YbMS and HfO_2 on the formation process of the TGO layer (described earlier), as YbMS/YbDS biphasic coatings without HfO_2 chipped off after 1–2

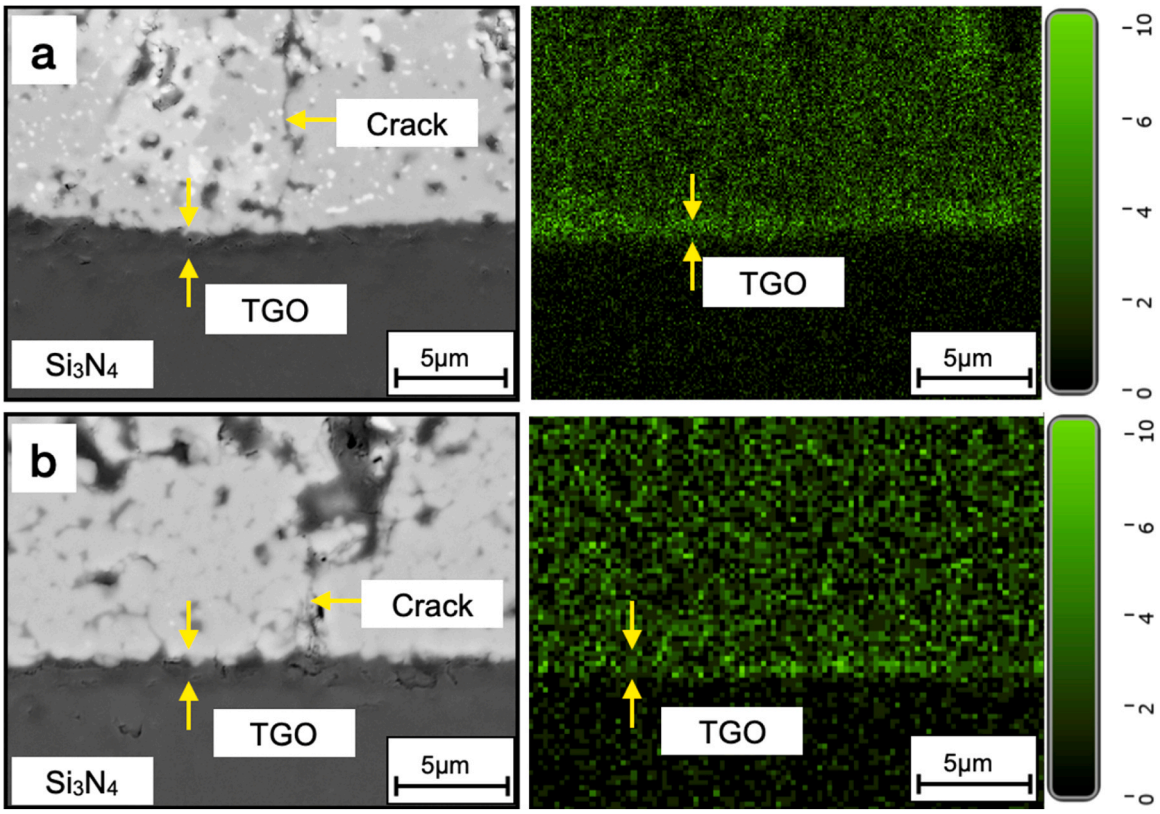

Fig. 12. SEM and EDS mapping of YbMS/YbDS+ 15HfO_2 coatings obtained via a – spraying and b – sedimentation technique.

Table 4
The microhardness values of the EBC were obtained by spraying and sedimentation, GPa.

	Spraying	Sedimentation
YbDS+ 15HfO_2	5.0 ± 0.3	3.4 ± 0.3
YbMS/YbDS+ 15HfO_2	4.3 ± 0.4	2.3 ± 0.2

cycles.

Fig. 13a and b show the surfaces of coatings obtained by spraying and sedimentation methods after 5 and 20 thermal shock experiments, respectively. The analysis of the samples revealed partial destruction or cracking of the coatings in areas containing defects that arose during the coating process. However, in case the coating is applied uniformly and the substrate surface is defect-free, it can withstand multiple thermocycling without damage. For instance, in Fig. 13b, after the first cycle, a crack was formed in the substrate and led to the destruction of the sample in subsequent thermocycling. Nevertheless, even after 20 cycles, there was no oxidation along the crack boundary, and no delamination of the coating was observed in this area. The experiment showed that the coating obtained by sedimentation with a silicon deficiency at the surface of the substrate leads to the formation of heat-resistant EBC. But, in the case of a Yb_2O_3:2SiO_2 ratio slurry sedimentation on the substrate, YbDS is formed, which does not react with the TGO formed on the surface. Hence, TGO is formed between EBC and Si_3N_4, which leads to the formation of bubbles on the EBC surface (Fig. 13b).

A more comprehensive analysis of coating failure following thermal cycling was conducted using SEM (Fig. 14a-d). The crack healing process was observed for YbMS/YbDS+ 15HfO_2 coatings obtained by the spraying method as shown in Fig. 14b. This could be attributed to the reaction of YbMS with SiO_2, subsequently leading to the formation of the YbDS phase with an increase in volume. This self-healing process contributes to the partial restoration of the coating and the alteration of the crack path, thereby enhancing the durability of the EBC. The results obtained are consistent with the research of Paksoy et al. [12], in which YbMS/YbDS coatings obtained via APS also exhibit self-healing ability.

The gradient EBC obtained through the sedimentation method in contrast to the homogenous EBC obtained using the spraying method exhibited a lower tendency for self-healing. This could be attributed to the presence of the top layer of HfO_2. However, even in this case, partial healing of minor cracks was observed as shown in Fig. 14c-d. Nevertheless, SEM analysis of the cross-section of the coatings confirmed that only large cracks reach the surface of the substrate, while all small cracks have a depth of up to 5 μm (Fig. 15).

Fig. 15 illustrates an SEM image of the YbMS/YbDS+ 15 HfO_2 coatings cross-section obtained via spraying and sedimentation after 20 thermal cycles ranging from 1200 °C to 20 °C. The cross-sectional analysis of the coatings revealed the formation of a narrow TGO layer (2.0–2.3 μm) at the site of a crack reaching the Si_3N_4 surface. Notably, partial healing of the crack was observed during thermal processing, with the presence of the YbDS phase along the entire length of the crack. Throughout the entire EBC-substrate contact zone, a consistent layer of YbDS, 2–3 μm thick, was also observed (Fig. 15a). This layer exhibited a relative deficiency of HfO_2 compared to the rest of the EBC volume. This leads to the hypothesis that HfO_2 diffuses into the TGO layer, modifying it, and thereby preventing the TGO layer thickness from reaching a critical value, which in turn avoids complete spallation of the EBC. Similar trends in TGO layer reduction when modified with Al_2O_3 in the Si bond coat have been observed in the researches [43,44]. The coating obtained by the sedimentation method also demonstrated high resistance to thermal shocks. Here, a similar formation of a 2.3 μm thick TGO layer was observed. However, no significant healing of deep cracks was noted.

Thermal cycling experiments confirmed the reliability of YbMS/YbDS+ 15HfO_2 coating without a Si bond coat. It should be noted that the main advantage of coatings without a Si bond coat is a higher operating temperature. Since the Si has a melting point (1410 °C). It is a

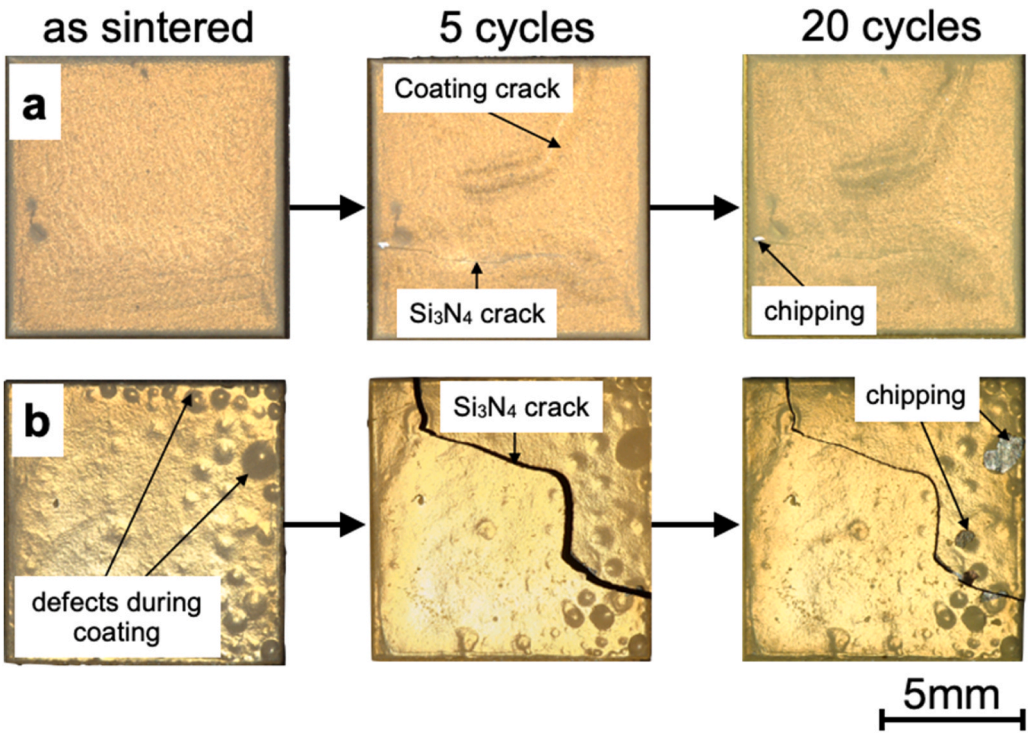

Fig. 13. Optical microscope images of YbMS/YbDS+ 15HfO_2 coatings (a – spraying and b- sedimentation) on Si_3N_4 substrate subjected to thermal cyclings after 0, 5 and 20 cycles with a temperature range from 1200 °C to 20 °C.

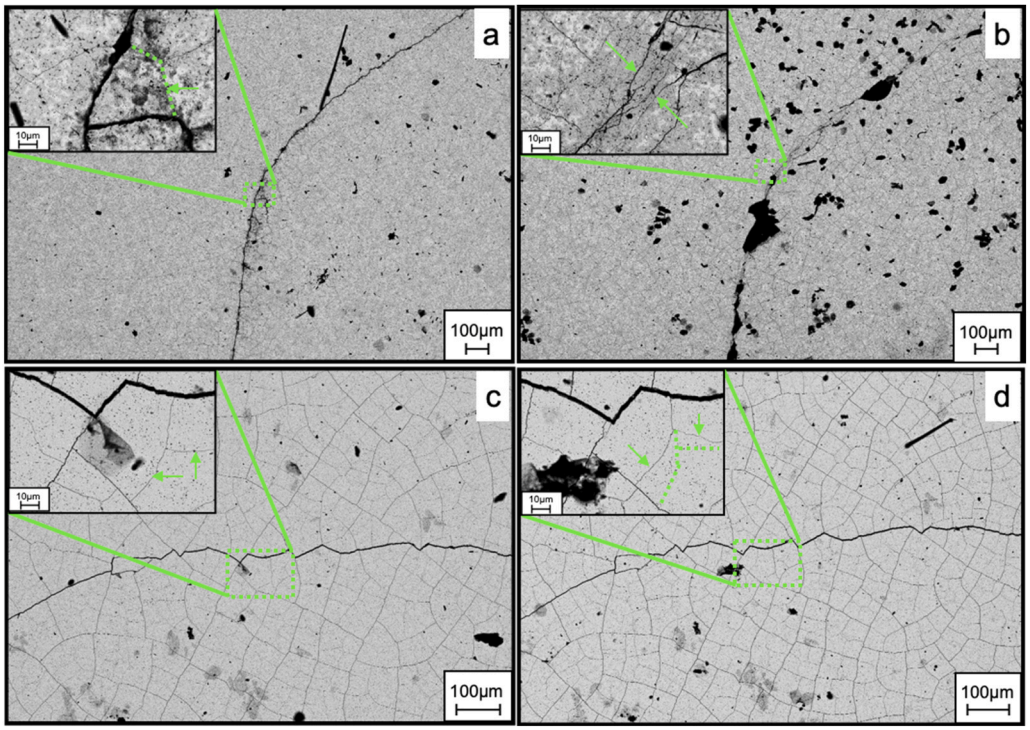

Fig. 14. BSE micrographs of YbMS/YbDS+ 15HfO_2 coatings obtained via spraying a - after 5 cycles, b – after 20 cycles and sedimentation c - after 5 cycles, d – after 20 cycles, a temperature range from 1200 °C to 20 °C.

limitation of the maximal operation temperature of the existing EBC. However, additional research and comparison of the coatings' properties are necessary. It is plausible that the incorporation of a reinforcing component in the form of whiskers could enhance the crack resistance of the gradient coating. While quantitative self-healing metrics were not recorded here, literature suggests reporting crack-width reduction ratios, healed-crack fractions, and healing rates under isothermal holds or cycles; YbMS-rich regions facilitate healing via SiO_2 consumption to form YbDS, whereas HfO_2-rich top layers can limit oxygen/water access and thus slow healing kinetics [12,38].

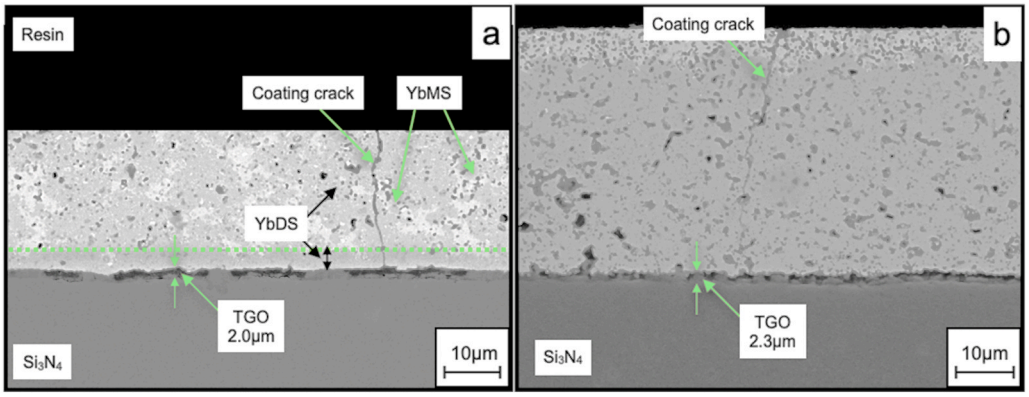

Fig. 15. BSE micrographs of YbMS/YbDS+ 15HfO_2 cross-section obtained via a – spraying and b – sedimentation after 20 cycles with a temperature range from 1200 °C to 20 °C.

3.3. Comparison with state-of-the-art EBCs and long-term oxidation behavior in water vapor

Recent work on Yb_2SiO_5–$Yb_2Si_2O_7$ gradient EBCs over Si–HfO_2 bond coats (APS) in 90 % H_2O–10 % O_2 at 1300 °C quantified TGO growth with a parabolic law $h(t) = k\ t^{1/2} + b$ and showed that increasing Yb_2SiO_5 content reduces corrosion rates and delays delamination; a gradient topcoat achieved a thinner TGO after 100 h (≈18.5 μm) than $Yb_2Si_2O_7$-rich single layers, while maintaining strong adhesion through reduced residual tensile stress [38]. Our PDC approach similarly targets low TGO growth by (I) eliminating Si bond coats to suppress interfacial SiO_2 formation, (II) distributing HfO_2 uniformly or as a surface-enriched gradient to act as a TBC and diffusion barrier, and (III) leveraging YbMS/YbDS biphasic compositions to consume excess SiO_2 in-situ. Although our present tests emphasize thermal cycling, future long-duration exposures (e.g., 90 % H_2O–10 % O_2, 1200–1300 °C, 10–100 h) should be used to extract parabolic rate constants and benchmark against [38], while also mapping ridge-/pit-like corrosion morphologies and phase evolution. Regarding thickness, the literature indicates that ~200 μm topcoats (APS) balance durability and stress, whereas our PDC coatings (50–100 μm) reduce mismatch but may be more permeable; gradient architectures can bridge this gap by tailoring composition through thickness to lower tensile stress and crack susceptibility [38]. For scale-up, PDC spraying is well-suited to complex shapes and large areas, whereas sedimentation enables reproducible gradients provided slurry rheology and particle-size distributions are tightly controlled; drying/pyrolysis protocols must minimize cracking and ensure uniform densification.

4. Conclusion

In this research, we explored the synthesis of $Yb_2Si_2O_7$-based EBCs integrated with HfO_2 using polymer-derived ceramics (PDC) technology. We implemented two approaches for applying these coatings, focusing on uniform and gradient HfO_2 distribution. These techniques included spraying and sedimentation on Si_3N_4 substrates without a Si bond coat. Our key findings include:

1. $Yb_2Si_2O_7$ coatings with HfO_2 additives without employing a Si bond coat were successfully synthesized by a spraying method. An increase in HfO_2 content resulted in a significant reduction in the grain size of the coating, from 10 μm in pure $Yb_2Si_2O_7$ to 0.5 μm in the $Yb_2Si_2O_7$ + 15 mol% HfO_2 composite coating. We propose a mechanism for the formation of SiO_2 along the $Yb_2Si_2O_7$ grain boundaries, originating from the oxidation of the Si_3N_4 (or/and Si bond coat) surface during sintering, leading to SiO_2 formation and shifting the Yb_2O_3-SiO_2 system's equilibrium.
2. The uniform and gradient composite coatings of $Yb_2Si_2O_7$ + 15 mol % HfO_2 were obtain in situ. These coatings demonstrated strong adhesion to the Si_3N_4 substrate without a Si bond coat (30 – 38 MPa). The spraying resulted in a uniform distribution, the sedimentation method led to a gradient HfO_2 distribution. However, the coatings exhibited relatively different hardness, laying from 5.0 ± 0.3 GPa to 3.4 ± 0.3 GPa for sprayed and sedimentated coatings, respectively.
3. The challenge of SiO_2 formation at $Yb_2Si_2O_7$ boundaries in the coating was effectively addressed. Yb_2SiO_5/$Yb_2Si_2O_7$ + HfO_2 composite coatings were produced by both spraying and sedimentation methods. These coatings were free of SiO_2 along the grain boundaries, achieved by applying a Si-deficit suspension, corresponding to the formation of Yb_2SiO_5/$Yb_2Si_2O_7$ in a 1:1 ratio. The excess SiO_2 formed during sintering contributed to the formation of $Yb_2Si_2O_7$, eliminating the TGO layer at the EBC-substrate interface and among $Yb_2Si_2O_7$ grains. This led to an increase in adhesion strength up to 42.6 MPa. The composite coating demonstrated remarkable stability during thermocycling tests, enduring up to 20 thermal cycles. The observed self-healing mechanism, which occurs during oxidation and SiO_2 formation, facilitates the reaction with Yb_2SiO_5, leading to the formation of $Yb_2Si_2O_7$ and enhancing the coating's durability.
4. Relative to state-of-the-art gradient Yb_2SiO_5/ $Yb_2Si_2O_7$ EBCs over Si–HfO_2 bond coats, our Si-bond-coat-free, PDC-fabricated coatings offer complementary advantages (suppressed interfacial SiO_2, tunable HfO_2 distribution). To fully quantify long-term oxidation resistance and self-healing, future work should measure TGO thickness vs time in 90 % H_2O–10 % O_2 at 1200–1300 °C, fit parabolic growth constants, and report standardized healing metrics (crack-width reduction, healed fraction, healing rate), enabling direct comparison with [38].

CRediT authorship contribution statement

Dmitrii Titov: Writing – original draft, Visualization, Validation, Methodology, Investigation, Formal analysis, Data curation. **Günter Motz:** Writing – review & editing, Writing – original draft, Validation, Supervision, Resources, Project administration, Methodology, Investigation, Funding acquisition, Formal analysis, Data curation, Conceptualization. **Stefan Schafföner:** Writing – review & editing, Writing – original draft, Visualization, Validation, Supervision, Resources, Methodology, Investigation, Conceptualization. **Eranezhuth Wasan Awin:** Writing – review & editing, Visualization, Validation, Methodology, Investigation, Formal analysis, Data curation.

Declaration of Competing Interest

The authors declare that they have no known competing financial interests or personal relationships that could have appeared to influence

the work reported in this paper.

Acknowledgements

The authors thank DFG (Deutsche Forschungsgemeinschaft) for the financial support within the project Mo 851/20–1 – AO675133.

Appendix A. Supporting information

Supplementary data associated with this article can be found in the online version at doi:10.1016/j.jeurceramsoc.2025.117932.

Data Availability

The data that support the findings of this study are available from the corresponding author upon reasonable request.

References

[1] T.M. Pollock, S. Tin, Nickel-based superalloys for advanced turbine engines: chemistry, microstructure and properties, J. Propuls. Power 22 (2006) 361–374.
[2] S. Cruchley, H. Evans, M. Taylor, An overview of the oxidation of Ni-based superalloys for turbine disc applications: surface condition, applied load and mechanical performance, Mater. High. Temp. 33 (2016) 465–475.
[3] A.G. Evans, J.W. Hutchinson, The mechanics of coating delamination in thermal gradients, Surf. Coat. Technol. 201 (2007) 7905–7916.
[4] B.T. Richards, H.N.G. Wadley, Plasma spray deposition of tri-layer environmental barrier coatings, J. Eur. Ceram. Soc. 34 (2014) 3069–3083.
[5] D.S. Fox, E.J. Opila, Q.N. Nguyen, D.L. Humphrey, S.M. Lewton, Paralinear oxidation of silicon nitride in a water-vapor/oxygen environment, J. Am. Ceram. Soc. 86 (2003) 1256–1261.
[6] H. Klemm, Silicon nitride for high-temperature applications, J. Am. Ceram. Soc. 93 (2010) 1501–1522.
[7] K.N. Lee, D.S. Fox, N.P. Bansal, Rare earth silicate environmental barrier coatings for SiC/SiC composites and Si3N4 ceramics, J. Eur. Ceram. Soc. 25 (2005) 1705–1715.
[8] M. Fritsch, H. Klemm, M. Herrmann, B. Schenk, Corrosion of selected ceramic materials in hot gas environment, J. Eur. Ceram. Soc. 26 (2006) 3557–3565.
[9] Ueno, S., Jayaseelan, D.D., Ohji, T. & Lin, H.-T. Corrosion and oxidation behavior of ASiO4 (A= Ti, Zr and Hf) and silicon nitride with an HfSiO4 environmental barrier coating. in 2005.
[10] S. Ueno, D.D. Jayaseelan, H. Kita, T. Ohji, H.T. Lin, Comparison of water vapor corrosion behaviors of Ln2Si2O7 (Ln=5Yb and Lu) and ASiO4 (A=Ti, Zr and Hf) EBC's, Key Eng. Mater. 317–318 (2006) 557–560.
[11] D. Tejero-Martin, C. Bennett, T. Hussain, A review on environmental barrier coatings: History, current state of the art and future developments, J. Eur. Ceram. Soc. 41 (2021) 1747–1768.
[12] A.H. Paksoy, P. Xiao, Study on sintering behaviour of ytterbium disilicate and ytterbium monosilicate for environmental barrier coating applications, Ceram. Int. 48 (2022) 11238–11250.
[13] Z. Zhang, et al., Research status of bond coats in environmental barrier coatings, Int. J. Appl. Ceram. Technol. 19 (2022) 1841–1859.
[14] M. Lu, H. Xiang, Z. Feng, X. Wang, Y. Zhou, Mechanical and thermal properties of Yb2SiO5: a promising material for T/EBCs applications, J. Am. Ceram. Soc. 99 (2016) 1404–1411.
[15] E. Garcia, O. Sotelo-Mazon, C.A. Poblano-Salas, G. Trapaga, S. Sampath, Characterization of Yb2Si2O7–Yb2SiO5 composite environmental barrier coatings resultant from in situ plasma spray processing, Ceram. Int. 46 (2020) 21328–21335.
[16] K.N. Lee, et al., Upper temperature limit of environmental barrier coatings based on mullite and BSAS, J. Am. Ceram. Soc. 86 (2003) 1299–1306.
[17] K.N. Lee, Yb $_2$ Si $_2$ O $_7$ Environmental barrier coatings with reduced bond coat oxidation rates via chemical modifications for long life, J. Am. Ceram. Soc. 102 (2019) 1507–1521.
[18] B.T. Richards, et al., Response of ytterbium disilicate–silicon environmental barrier coatings to thermal cycling in water vapor, Acta Mater. 106 (2016) 1–14.
[19] A.J. Leadbetter, A.F. Wright, The α—β transition in the cristobalite phases of SiO $_2$ and AlPO $_4$ I. X-ray studies, Philos. Mag. 33 (1976) 105–112.
[20] R.C. Breneman, J.W. Halloran, A. Arbor, Hysteresis upon repeated cycling through the beta-alpha cristobalite transformation, J. Ceram. Sci. Technol. 6 (2015) 55–61.
[21] E. Bourova, P. Richet, Quartz and Cristobalite: high-temperature cell parameters and volumes of fusion, Geophys Res Lett. 25 (1998) 2333–2336.
[22] Zhu, D. Aerospace Ceramic Materials: Thermal, Environmental Barrier Coatings and SiC/SiC Ceramic Matrix Composites for Turbine Engine Applications, 2018.
[23] K.N. Lee, Protective coatings for gas turbines, Gas. Turbine Handb. 4 (2006).
[24] R.R. Naslain, SiC–Matrix Composites: Tough Ceramics for Thermostructural Application in Different Fields. Engineered Ceramics, Wiley, 2016, pp. 142–159, https://doi.org/10.1002/9781119100430.ch8.
[25] A.L. Robertson, F. Solá, D. Zhu, J. Salem, K.W. White, Microscale fracture mechanisms of HfO2-Si environmental barrier coatings, J. Eur. Ceram. Soc. 39 (2019) 2409–2418.
[26] R. Anton, V. Leisner, P. Watermeyer, M. Engstler, U. Schulz, Hafnia-doped silicon bond coats manufactured by PVD for SiC/SiC CMCs, Acta Mater. 183 (2020) 471–483.
[27] Kowalski, B., Fox, D. & Jacobson, N.S. Water Vapor Corrosion in EBC Constituent Materials. in Pacific Rim Conference on Ceramic and Glass Technology (PACRIM, 2017.
[28] J.T. Gaskins, et al., Review—investigation and review of the thermal, mechanical, electrical, optical, and structural properties of atomic layer deposited high-k dielectrics: beryllium oxide, aluminum oxide, hafnium oxide, and aluminum nitride, ECS J. Solid State Sci. Technol. 6 (2017) N189.
[29] Z. Zhang, et al., High-temperature oxidation performance of novel environmental barrier coating 50HfO2-50SiO2/YxYb(2−x)Si2O7 at 1475 °C, J. Eur. Ceram. Soc. 43 (2023) 1127–1140.
[30] S. Xiao, et al., Exploration of the oxidation behavior and doping ratio of the Si–HfO $_2$ bond layer used in environmental barrier coatings, Int J. Appl. Ceram. Technol. 20 (2023) 1753–1763.
[31] N.S. Jacobson, Corrosion of silicon-based ceramics in combustion environments, J. Am. Ceram. Soc. 76 (1993) 3–28.
[32] B.J. Harder, Oxidation performance of Si-HfO2 environmental barrier coating bond coats deposited via plasma spray-physical vapor deposition, Surf. Coat. Technol. 384 (2020) 125311.
[33] S. Bernard, Design, Processing, and Properties of Ceramic Materials from Preceramic Precursors, Nova Science Publishers, 2012.
[34] G. Barroso, Q. Li, R.K. Bordia, G. Motz, Polymeric and ceramic silicon-based coatings – a review, J. Mater. Chem. A Mater. 7 (2019) 1936–1963.
[35] D.D. Jayaseelan, S. Ueno, T. Ohji, S. Kanzaki, Sol–gel synthesis and coating of nanocrystalline Lu2Si2O7 on Si3N4 substrate, Mater. Chem. Phys. 84 (2004) 192–195.
[36] M. Lenz Leite, U. Degenhardt, W. Krenkel, S. Schafföner, G. Motz, In situ generated Yb2Si2O7 environmental barrier coatings for protection of ceramic components in the next generation of gas turbines, Adv. Mater. Interfaces 9 (2022).
[37] D.L. Poerschke, J.S. Van Sluytman, K.B. Wong, C.G. Levi, Thermochemical compatibility of ytterbia–(hafnia/silica) multilayers for environmental barrier coatings, Acta Mater. 61 (2013) 6743–6755.
[38] S. Yu, et al., Yb2SiO5-Yb2Si2O7 gradient environment barrier coating: Rational design and corrosion behavior in water vapor environment at 1300 ℃, J. Eur. Ceram. Soc. 44 (2024) 6097–6112.
[39] G. Ziegler, et al., Synthesis, microstructure and properties of SiCN ceramics prepared from tailored polymers, Mater. Chem. Phys. 61 (1999) 55–63.
[40] J.A. Deijkers, H.N.G. Wadley, Hafnium silicate formation during the reaction of β-cristobalite SiO $_2$ and monoclinic HfO $_2$ particles, J. Am. Ceram. Soc. 103 (2020) 5400–5410.
[41] Z. Zhang, et al., Effect of the HfO2/SiO2 pre-mixing ratio and heating temperature on the formation of HfSiO4 as a bond coat of environmental barrier coatings, Ceram. Int. 48 (2022) 15657–15667.
[42] J.A. Deijkers, M.R. Begley, H.N.G. Wadley, Failure mechanisms in model thermal and environmental barrier coating systems, J. Eur. Ceram. Soc. 42 (2022) 5129–5144.
[43] K.N. Lee, A. Garg, W.D. Jennings, Effects of the chemistry of coating and substrate on the steam oxidation kinetics of environmental barrier coatings for ceramic matrix composites, J. Eur. Ceram. Soc. 41 (2021) 5675–5685.
[44] D. Chen, TGO growth behavior in environmental barrier coatings with modified silicon bond coat, J. Therm. Spray. Technol. 33 (2024) 174–180.